AJPR
Avicenna Journal of Pharmaceutical Research
Avicenna J Pharma Res. 2025;6(1):15-26
DOI: 10.53208/ajpr.6.1.15
http://ajpr.umsha.ac.ir



Original Article

Integrating Fragment-Based Design, Machine Learning, and Molecular Dynamics to Identify Selective Anticancer Peptides Targeting 14-3-3σ

Yasin Fahimi[1], Dara Dastan[2], Ahmad Ebadi[1*]

[1] Department of Medicinal Chemistry, School of Pharmacy, Medicinal Plants and Natural Products Research Center, Hamadan University of Medical Sciences, Hamadan, Iran
[2] Department of Pharmacognosy, School of Pharmacy, Medicinal Plants and Natural Products Research Center, Hamadan University of Medical Sciences, Hamadan, Iran

Article history:
Received: January 27, 2025
Revised: February 28, 2025
Accepted: May 1, 2025
Published: July 27, 2025

***Corresponding author:**
Ahmad Ebadi, Department of Medicinal Chemistry, School of Pharmacy, Medicinal Plants and Natural Products Research Center, Hamadan University of Medical Sciences, Hamadan, Iran
E-mail: a.ebadi@umsha.ac.ir
Tel: +988138381590

Abstract

Background: The modulation of disease-relevant protein–protein interactions (PPIs) using small-molecule inhibitors is an evolving strategy in drug discovery. The 14-3-3 protein family engages in nearly 700 PPIs, making its members attractive therapeutic targets in a wide range of diseases. Among them, 14-3-3σ is closely associated with cancer initiation and progression, and its overexpression has been reported in gallbladder, liver, and breast cancers. The highly conserved amphipathic groove of 14-3-3σ is essential for mediating PPIs involved in cell-cycle regulation. Anticancer peptides (ACPs) have therefore emerged as promising PPI modulators for the treatment of related malignancies.

Methods: In the present study, we designed a library of 1,059,049 putative ACPs targeting 14-3-3σ using a fragment-based peptide design strategy integrated with a machine-learning (ML) predictor. A total of 198 high-scoring peptides were docked into the amphipathic groove of 14-3-3σ. The selected peptides were synthesized via solid-phase peptide synthesis and characterized by RP-HPLC and LC–MS.

Results: Subsequent molecular docking, long coarse-grained molecular dynamics (CG-MD), and all-atom MD simulations identified two hexapeptides, p8 (FRRVFN) and p9 (FRRWRN), with the strongest binding energies (−70.7 and −80.3 kcal.mol^{-1}, respectively). *In vitro* cytotoxicity assays against MCF-7 cells demonstrated potent anticancer activity, with IC_{50} values of 127.1±9.3 µM for p8 and 12.3±1.7 µM for p9.

Conclusion: Overall, this study demonstrates that integrating fragment-based peptide design with ML predictions and MD simulations provides an efficient and reliable strategy for identifying potent ACPs targeting 14-3-3σ.

Keywords: 14-3-3σ; Anticancer peptide, Fragment-based peptide design, Machine Learning, MD simulation, Protein-protein interaction

Introduction

Direct interactions between proteins in protein networks are vital for regulating cell functions. Protein-protein interactions (PPIs) establish an emerging network that affects all cellular processes [1, 2]. Disruptions in the interconnected network of PPIs could cause metabolic diseases, malignancies, and

© 2025 The Author(s); Published by Hamadan University of Medical Sciences. This is an open-access article distributed under the terms of the Creative Commons Attribution License (http://creativecommons.org/licenses/by/4.0), which permits unrestricted use, distribution, and reproduction in any medium, provided the original work is properly cited.

[Downloaded from ajpr.umsha.ac.ir on 2026-11-06]

[DOI: 10.53208/ajpr.6.1.15]

inflammation [3]. PPIs have been recognized as therapeutic targets of great interest in drug design projects [4]. Despite challenges, such as highly dynamic and expansive interfacial areas of receptors, modulating disease-relevant PPIs is an evolving approach [5]. In this regard, therapeutic interventions for modulating abnormal PPIs have been developed. Nowadays, these modulators are present in clinical trials and even on the market [6].

Protein-protein interactions within the 14-3-3 (YWHA) protein family are a major focus of research due to their critical roles in numerous cellular processes. In mammals, seven isoforms exist (α/β, γ, σ, δ/ζ, η, ε, τ), all of which are highly conserved and ubiquitously expressed in eukaryotes [7, 8]. These proteins regulate a vast array of signaling pathways involved in cell cycle control, metabolism, apoptosis, inflammation, and protein trafficking [9]. The 14-3-3 family is implicated in neurological disorders, cancer, aging, and cellular homeostasis. They function by binding to diverse signaling proteins, such as Raf kinases, Cdc phosphatase, YAP, and p53 [9]. This functional versatility makes 14-3-3 proteins promising therapeutic targets, particularly for cancer [10]. Their interactions can be modulated by small molecules, peptides, and peptidomimetics [11].

The 14-3-3 modulators bind to an amphipathic groove involving specific, highly conserved residues—Lys49, Arg56, Tyr127, and Tyr129—which are critical for the binding of protein partners. [12]. The 14-3-3σ is more strongly associated with malignancy and cell cycle regulation than other isoforms in the family [13]. The 14-3-3σ is a unique isoform and, unlike the other isoforms, is stable only as a homodimer [14, 15]. Met202, Asp204, and His206 residues are unique in 14-3-3σ [16]. The 14-3-3σ is directly involved in the inspection of G2/M-phase by protecting the tumor-suppressing factor against degradation and binding to MDM2 [17]. 14-3-3σ is also a kinase-dependent inhibitor and regulates the antiproliferative activity of transforming growth factor beta-1 (TGF-β1) through a Smad-dependent mechanism [9]. In addition, reports show that 14-3-3σ controls cell proliferation and cancer metastasis by terminating the NF-κB signal in breast cells and regulating nuclear export of the p65 subunit of the NF-κB transcription factor, ultimately inhibiting its transcriptional activity [18]. Despite insights into the specific roles of 14-3-3σ within protein-protein interaction networks, designing and developing selective modulators remains a significant challenge. Over the past decade, various non-selective modulators of 14-3-3σ have been reported [12].

A new class of supramolecular peptide-based ligands stabilizes 14-3-3 and Estrogen Receptor alpha (ERα) PPIs (Figure 1). ERα has a central role in the majority of breast cancers, and the 14-3-3 proteins negatively regulate ERα. Consequently, stabilizing the 14-3-3/ERα PPI is an interesting strategy in developing new anticancer agents [19].

The 14-3-3σ mediates the expression of MMP-1 via 14-3-3σ/APN (aminopeptidase N) PPIs. The upregulation of MMP-1 is associated with abnormal cell growth. The phosphonic acid derivative 2 (Figure 1) is the extracellular inhibitor of 14-3-3σ against APN (IC_{50}=5 μM) [20]. A phosphonate tweezer-like molecule (Figure 3 and 1) can bind near the central channel of 14-3-3 and modulate PPI interactions with C-Raf and ExoS [21]. The pyrazol-3-one derivative (Figure 4 and 1) shows significant cytotoxicity (LD_{50}=1.04 μM) against Ba/F3 cells. Compound 4 was discovered by an *in silico* structure-based approach as an inhibitor of 14-3-3/c-Abl PPIs [22].

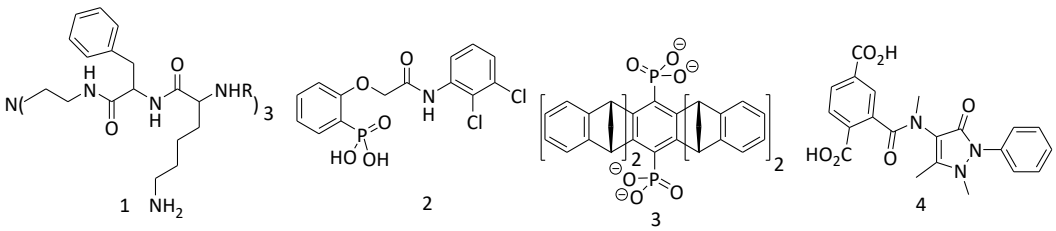


Figure 1. Chemical structures of 14-3-3 modulators. Both acidic and basic molecules could interact with the amphipathic groove. Negatively charged functional groups form salt bridges with positively charged Arg residues. Conversely, positively charged functional groups form the same bonds with the phospho-accepting pocket in the amphipathic groove. Nevertheless, notice that effective non-peptidic 14-3-3 modulators contain functional groups that reduce their drug-likeness. This is an important factor that increases the attrition rate of 14-3-3 modulators during further evaluation.

[Downloaded from ajpr.umsha.ac.ir on 2026-11-06]

[DOI: 10.53208/ajpr.6.1.15]

Peptides are the preferred candidates for modulation of PPIs rather than small molecules. Peptides are capable of closely imitating the principal PPIs [6]. A 20-residue peptide (PHCVPRDLSWLDLEANMCLP) was discovered using the phage display technique. This peptide is the first peptidic non-selective inhibitor of 14-3-3s. The middle sequence (bold amino acids containing an Asp residue) binds to Arg56 and Arg127 of the phospho-accepting pocket in the amphipathic groove. The C-terminal Leu forms vdW interactions with Gly169 and Ile217 [23]. Inhibition of the p53-SFN complex leads to decreased expression of cyclin B1 and CDC2 in RWP1 and Mia Paca-2 cells. The TEGPDSD peptide inhibits the p53-SFN complex, leading to cell death by affecting the cell cycle, especially in the G2 phase [24]. In a recent study, a cyclotide plant secondary metabolite (CGETCVGGTCNTPGCKCSWPVCTRNGLPV) stabilizes the 14-3-3/Foxo3a complex and consequently inhibits the Foxo3a function. This natural peptide also stabilizes the complex of 14-3-3s with Tau and C-Raf [25]. The anionic area in the binding pocket of 14-3-3σ is a favored binding region for positive peptidic inhibitors. MARHpSYPA peptide, an octapeptide containing a phosphoserine residue, inhibits 14-3-3σ by occupying two amphipathic binding regions of 14-3-3σ, with remarkable suppression in a prostate cancer cell line [26].

The 14-3-3σ modulators have been extensively explored as potential anticancer agents; however, no related drugs have yet reached clinical application. Peptides are effective modulators of protein–protein interactions, but no rationally designed peptidic modulators of 14-3-3σ have been reported to date. In this study, novel peptidic inhibitors of 14-3-3σ were designed and synthesized. An in-silico fragment-based approach was used to generate an initial peptide library, followed by supervised machine learning (ML), molecular docking, and 500-ns coarse-grained molecular dynamics (CG-MD) simulations to identify the most promising candidates. Two hexapeptides were subsequently synthesized and evaluated in vitro for antiproliferative activity, demonstrating the effectiveness of the proposed design strategy.

Materials and Methods

Chemicals

Fmoc amino acids comprising Fmoc-Phe-OH, Fmoc-Arg (Pbf)–OH, Fmoc-Asn(Trt)–OH, Fmoc-Trp (Boc)–OH, Fmoc-Val-OH, and 2-(1H-benzotriazole-1-yl)-1,1,3,3- tetramethyluronium hexafluorophosphate (TBTU) were purchased from GL Biochem (China). The 2-chlorotrithyl chloride resin, *N*, *N*-diisopropylethylamine (DIPEA), trifluoroacetic acid (TFA), triisopropylsilane (TIS), diethyl ether, *N*, *N*-dimethylformamide (DMF), and dichloromethane (DCM) were bought from Merck Chemical Co. The standard MTT [3-(4,5-dimethylthiazol-2-yl)-2,5 diphenyltetrazolium bromide], FBS (fetal bovine serum), penicillin, and streptomycin were purchased from Biosera (Austria). Moreover, MCF-7, MDA-MB-231, and HEK293 cell lines were obtained from the National Cell Bank of Iran, Pasteur Institute, Tehran, Iran.

Molecular modeling

The 14-3-3σ crystallographic structure in complex with the AHSpSPASLQ phosphopeptide was obtained from the RCSB Protein Data Bank (PDB code: 6G8I) [27]. The crystallographic structure was selected based on the structural integrity (without missing residues), resolution (1.6 Å), mutation (no), and the organism (Homo sapiens).

Fragment-based peptide design

Fragment-based docking was conducted using the SEED program [28]. The fragments of 20 natural amino acids (see Figure 2) were docked into the amphipathic binding groove of 14-3-3σ. Fragments corresponding to the 20 natural amino acids were docked into the amphipathic binding groove of 14-3-3σ. The receptor was parameterized with the CHARMM27 force field [29], while fragments used the CHARMM general force field (CGenFF) [30]. The binding site was defined as a 15 Å radius sphere centered on the Cα atom of Asp226, selected via alanine scanning as a key residue. This radius encompassed all relevant binding site amino acids. The SEED accounts for electrostatic desolvation effects using a generalized Born approach, with dielectric constants set at 2.0 for the solute and 78.5 for the solvent.

[Downloaded from ajpr.umsha.ac.ir on 2026-11-06]

[DOI: 10.53208/ajpr.6.1.15]

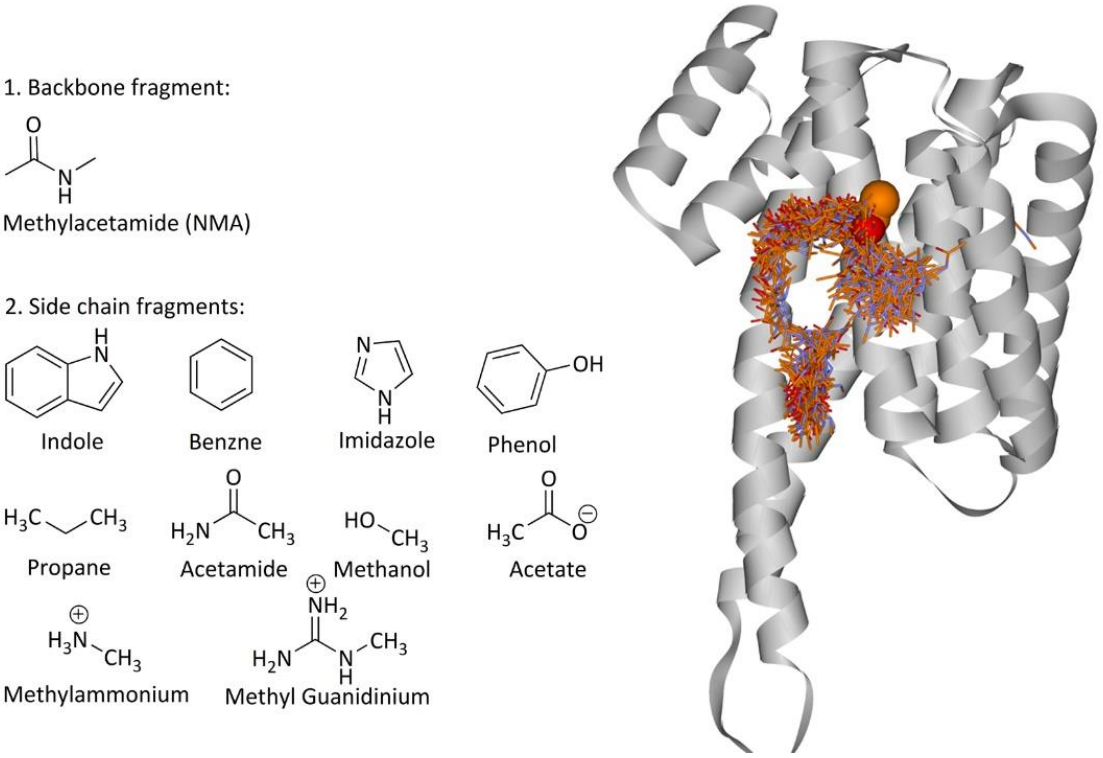


Figure 2. Chemical structure of 11 fragments was obtained from the dissection of 15 natural amino acid residues. The basic (Arg, Lys) and acidic (Asp, Glu) residues were considered in ionized form. The orientation and distribution of NMA fragments (orange stick) at the amphipathic groove of 14-3-3σ (gray flat ribbon) are shown. The best-scoring NMA fragment is shown in orange CPK.

N-methylacetamide (NMA) fragments with the best docking scores were used to design possible peptide backbones. Side-chain fragments were then selected and assigned to corresponding amino acids based on their distance to the Cα of the NMA and their binding energy. Since an NMA could sometimes be assigned to multiple amino acids, permutations were used to generate all possible peptide sequences, resulting in a final designed library of 1,059,049 peptide chains.

Machine learning

An ML approach was utilized to discriminate between anticancer peptides (ACPs) and non-anticancer peptides (non-ACPs) in the designed peptide library. Machine learning models were constructed in Python v2.7 using the Scikit-Learn v1.1.1 library. A supervised predictive NN model was trained using ACPs and non-ACPs whose effects have already been proven. A library of 568 ACPs and 867 non-ACPs was collected from CancerPPD and RCSB [31]. Molecular properties, including pepCATS (*Chemically Advanced Template Search*) pharmacophore feature descriptors [32], Eisenberg's hydrophobicity, Eisenberg's hydrophobic moment [33], charge, density, and peptide length (number of residues), were used to represent the peptide sequences. Low-variance features were removed from the dataset. Between features with high covariance, only one of them was kept in the dataset. We trained the model using 80%, 10%, and 10% of all data for training, validation, and testing, respectively. Logistic regression was used as the classification algorithm, with a learning rate of 0.001 and 50 epochs. Accuracy ($\frac{TN+TP}{TP+TN+FP+FN}$), precision ($\frac{TP}{TP+FP}$), recall ($\frac{TP}{TP+FN}$), and F1 score ($2 \times \frac{recision*Recall}{recision+Recall}$) were calculated to evaluate the efficacy of the trained model.

Peptide-14-3-3σ molecular docking

Molecular docking studies were carried out by the AutoDock Vina program [34]. Peptides obtained from the previous step and 14-3-3σ PDBQT files were prepared by the AutoDockTools-1.5.4 program [34]. A cubic box with dimensions of 30×30×30 Å^3 with a lattice spacing of 1 Å was considered in the center of the amphipathic groove of the receptor.

[Downloaded from ajpr.umsha.ac.ir on 2026-11-06]

[DOI: 10.53208/ajpr.6.1.15]

The rest of the parameters were considered the same as the software defaults.

Coarse-grained MD (CG-MD) simulations

Coarse-grained MD (CG-MD) simulations were run using the Martini model and ElNeDyn22 force field [35]. The system (14-3-3σ and 14-3-3σ/peptides complexes) was solvated in a dodecahedral box containing about 36500 nonpolarizable water beads and neutralizing counterions, Na^+. The CG-MD simulations were run using GROMACS-2019.1 [36]. By employing the switch function, the vdW interaction was shifted from 9 to 12 Å, and the electrostatic interaction was set to 12 Å, with neighbor lists updated every 10 steps. Velocity-rescaling temperature coupling at 300 K and the Parrinello-Rahman barostat pressure coupling with a time coupling constant of 12 ps and a compressibility value of 3×10^{-4} bar^{-1} were applied to maintain a constant temperature and pressure, respectively [37]. A timestep of 20 fs was used. Neighbor lists were updated every 10 steps. Periodic boundary conditions in x, y, and z directions were used in all simulations. The energy minimization was performed for up to 5000 steps using the steepest descent. Afterward, the system was equilibrated for 10 ns by restraining the 14-3-3σ/14-3-3σ-peptide position before the production run. The production phase for 14-3-3σ and 14-3-3σ/peptides complexes were run for 0.5 µs.

Atomistic MD simulation

Atomistic MD simulations were carried out using the GROMACS package version 2019.1 with the standard GROMOS53A6 force fields on a Linux server [36]. The system was centered in a dodecahedron box with a 10 Å distance from the edges. The 14-3-3σ and 14-3-3σ/peptides complexes were solvated in the SPC water model. The system was neutralized with counter ions (Na^+ or Cl^- ions) at pH = 7.0. The long-range electrostatic interactions were calculated by the Particle Mesh Ewald (PME) method, and the short-range vdW interactions were truncated at 14 Å. The bond lengths were constrained using the linear constraint solver (LINCS) algorithm with an integration time step of 2 fs [38]. The energy minimization was performed using the steepest descent integrator. The systems were equilibrated at NVT (300 K) and NPT (1 bar) ensembles using the velocity rescaling algorithm and Parrinello-Rahman barostat for 200 and 500 ps, respectively [37]. The explicit MD simulations were performed for apo 14-3-3σ and peptide-14-3-3σ complexes. Trajectories were sampled at an interval of 2 ps. Finally, the GROMACS tools were used to evaluate MD trajectories.

Synthesis

The two peptides, FRRVFN and FRRWRN, were synthesized using the Fmoc solid-phase peptide synthesis (SPPS) method on 2-chlorotrityl chloride resin, proceeding from the C- to the N-terminus. The resin was washed alternately with DMF and DCM. Amino acid couplings were performed using TBTU and DIEA as activators. Fmoc deprotection was achieved with 20% piperidine in DMF, and coupling efficiency was monitored via the Kaiser test and UV spectroscopy. The peptides were cleaved from the resin using a TFA/H_2O/phenol/TIS (85:5:5:5 v/v%) cocktail and subsequently characterized by LC-MS and RP-HPLC.

Purification

The purification was performed on a reverse-phase HPLC (RP-HPLC-PDA, Waters) using a preparative column (Waters 2998 UV–vis detector, C18 column, 250 × 20 mm). A 65 min linear gradient of 10-100% CH_3OH in water and UV detection at 214 and 280 nm was used as the washing program. The analytical RP-HPLC-PDA was performed on a Shimadzu HPLC system (equipped with an LC-20AD XR pump and SPDM20A UV–vis detector) using a C18 column (250×4.6 mm). An LC-ESI-MS system was used to characterize the peptide chains.

Cell proliferation assay

An MTT assay was performed to evaluate the antiproliferative effects of the synthesized peptides. Cells were seeded in a 96-well plate ($3–5\times10^3$ cells/well) and incubated for 24 h at 37°C and 5% CO_2. The cells were then treated with varying concentrations of each peptide in triplicate for 72 h. Following incubation, the media were carefully removed, and 5 mg/ml MTT solution in PBS was added to each well. After a 4-hour incubation to

[Downloaded from ajpr.umsha.ac.ir on 2026-11-06]

[DOI: 10.53208/ajpr.6.1.15]

allow formazan crystal formation, 200 µl of DMSO was added per well and incubated in the dark for 20 min. The absorbance of the dissolved formazan was measured at 570 nm (with background correction at 650 nm) using a Bio-Rad 680 microplate reader. The IC_{50} values were determined by plotting log [concentration (µM)] against the percentage of cell viability. Each experiment was independently repeated 2–3 times.

Results and Discussion

Fragment-based peptide design, MD simulations, machine learning (ML), and protein–peptide docking were employed to model novel ACPs. This stepwise strategy successfully identified two peptides that matched the proposed ACP pharmacophore. The amphipathic groove of 14-3-3σ, defined by its interaction with the AHSpSPASLQ phosphopeptide, was used as the docking site. Amino acid fragments were docked into this groove to evaluate their interactions across the binding site independently of the peptide backbone, enabling library design based on key fragment and NMA interactions. An iterative fragment-linking process generated a comprehensive peptide library, with residue selection guided by optimal binding interactions. To enrich for active candidates, a three-step filtering strategy was applied: ML-based screening, molecular docking based on binding energy and key interactions, and coarse-grained followed by atomistic MD simulations to assess long-term stability and atomic-level interactions. Two top-ranked hexapeptides were synthesized by SPPS and evaluated *in vitro* for cytotoxic activity after purification.

Fragment-based drug design

The fragment library comprised ten molecular fragments, each representing key functional groups of specific amino acids. This set modeled a total of 15 natural amino acids: Phenol (representing Tyr), Imidazole (representing His), Methylguanidinium (representing Arg), Propyl (representing Val, Ile, Leu), Acetamide (representing Asn, Gln), Methanol (representing Ser, Thr), Acetate (representing Asp, Glu), Methylammonium (representing Lys), Indole (representing Trp), Benzyl (representing Phe). The peptide backbone was represented by N-methylacetamide (NMA). Cysteine and methionine were excluded due to oxidation susceptibility. Glycine, alanine, and proline were omitted because their side chains are either too small (hydrogen or methyl) or, in the case of proline, introduce a cis-amide bond and a turn in the peptide chain.

All 11 fragments were docked into the amphipathic binding site of 14-3-3σ, targeting crucial residues Arg56, Arg129, and Tyr130. Backbone orientation was selected based on NMA orientation and binding energy. The backbone sequence was designed from the C- to the N-terminus by linking NMAs, with a gap exceeding 1.5 Å terminating the chain. This process resulted in the assignment of two hexapeptide backbones. Each NMA position was then assigned an amino acid based on the probability distribution of amino acid fragments around the Cα atom of the designed backbone. The fragment with the highest probability determined the final amino acid. Based on optimal distances between side chains and the backbone derived from optimized amino acid structures, residues were clustered: Class 1 (1.5 Å: Val, Ile, Ser, Thr, Asn, Asp); Class 2 (2.5 Å: Leu, Gln, Glu, Phe, Tyr, His, Trp); Class 3 (3.5 Å: Arg, Lys). Permutations were used for positions with equal probabilities among fragments, generating a library of 1,059,049 peptide sequences. To enrich this library for ACPs, an ML classifier was developed for subsequent filtering.

Machine learning

A binary ML classifier was trained to categorize the designed peptides into ACPs and AMPs based on amino acid sequence representations. The ML classifier was trained on “positive” (ACPs, active) and “negative” (non-ACPs, inactive) peptides. All amino acid sequences were represented numerically in a computer-readable form by the use of molecular descriptors. A combination of PEPCATS pharmacophore feature descriptors and four global properties, namely, Eisenberg’s hydrophobicity, Eisenberg’s hydrophobic moment, charge density, and peptide length (number of residues) was employed to represent each peptide as a numerical vector. The PEPCATS descriptor represents the amino acid sequences as binary vectors indicating cross-correlated pharmacophore features of the

[Downloaded from ajpr.umsha.ac.ir on 2026-11-06]

[DOI: 10.53208/ajpr.6.1.15]

individual amino acids (hydrophobic, aromatic, hydrogen-bond acceptor, hydrogen-bond donor, positively ionizable, negatively ionizable). The model was trained on 80% of the randomized data and validated and tested on 10% each. Data splitting was performed by stratified sampling, considering the length of the peptide as a deterministic parameter in the distribution of physicochemical properties. The performance of our classification model was assessed by the ROC curve, in which the area under the ROC curve was satisfactory (AUC=0.98). The performance of both classifiers exceeded 0.9 for both the training and the test data for all calculated metrics (Figure 3).

The performance of machine learning model

Metric	Train Score	Validation Score	Test Score
Accuracy	0.99	0.96	0.93
Precision	0.97	0.90	0.89
Recall	0.95	0.91	0.90
F1-score	0.96	0.90	0.89

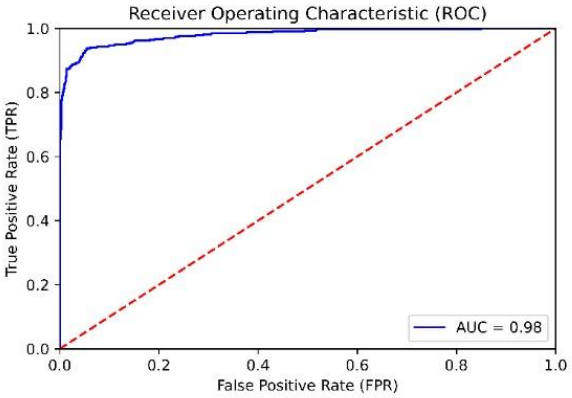


Figure 3. Performance of the binary classifier that was trained on ACPs and non-ACPs. The results

Table 1 presents the scores for the top 10 ranked hexapeptides from the designed library. Analysis of the peptide sequences and their scores revealed a prevalence of FRR, FR, and RR motifs. All high-ranking peptides contained at least two basic residues (arginine), typically in consecutive positions. Tryptophan emerged as the most frequent amino acid after arginine. Previous studies indicate that the presence of a positively charged residue pair and overall hydrophobicity are key features of ACPs [45].

Table 1. Sequence, predicted score, and free energy of binding (ΔG_b, kcal mol^{-1}) of 10 top-ranked peptides. The frequency of basic and hydrophobic amino acids was a feature of the designed library.

Peptide	Sequence	Score	ΔG_b (kcal mol^{-1})
p1	FRRFWN	0.91	-10.92
p2	RWLRQW	0.90	-10.85
p3	RFVRQW	0.89	-9.56
p4	RFWRQW	0.89	-9.79
p5	FRRFVN	0.89	-9.73
p6	RFLRQW	0.89	-9.17
p7	WRRVRN	0.89	-9.02
p8	FRRVFN	0.88	-10.00
p9	FRRWRN	0.88	-10.11
p10	WRRWRN	0.88	-8.90

Molecular docking

The top 1000 scoring peptides from an ML model were docked into the amphipathic binding groove. During subsequent filtering, both binding energy and interaction patterns with the 14-3-3δ groove interface were analyzed. After docking, peptides were ranked by binding energy (Table 1). P1 and p2 showed the highest binding energy, followed by p9 and p8, with marginal differences between the top contenders. Known key interface residues for 14-3-3σ binding include Glu39, Lys49, Arg56, Arg60, Arg129, Lys122, Tyr130, and Asn175.

The analysis revealed novel interactions: Ser45 formed hydrogen bonds and Pro16 engaged in van der Waals (vdW) interactions in high-affinity peptides, interactions not commonly reported before. In p1, Arg3 interacted via vdW forces with Lys49, Ser45, and Tyr130, and formed hydrogen bonds with Asp126, Lys122, and Tyr130. Trp6 had vdW contacts with Arg56, Asp226, and Arg129, plus a hydrogen bond with Glu182. In p2, Arg5 formed a hydrogen bond

[Downloaded from ajpr.umsha.ac.ir on 2026-11-06]

[DOI: 10.53208/ajpr.6.1.15]

with Tyr130 and Glu182, and vdW interactions with critical residues Lys122 and Arg129.

A consistent feature among the top 10 peptides was hydrogen bonding with the key residue Tyr130. Interactions with Asn42 were also notable. Interestingly, Ser45—not previously identified as a key residue—formed hydrogen bonds with peptides p8 (one bond) and p9 (two bonds).

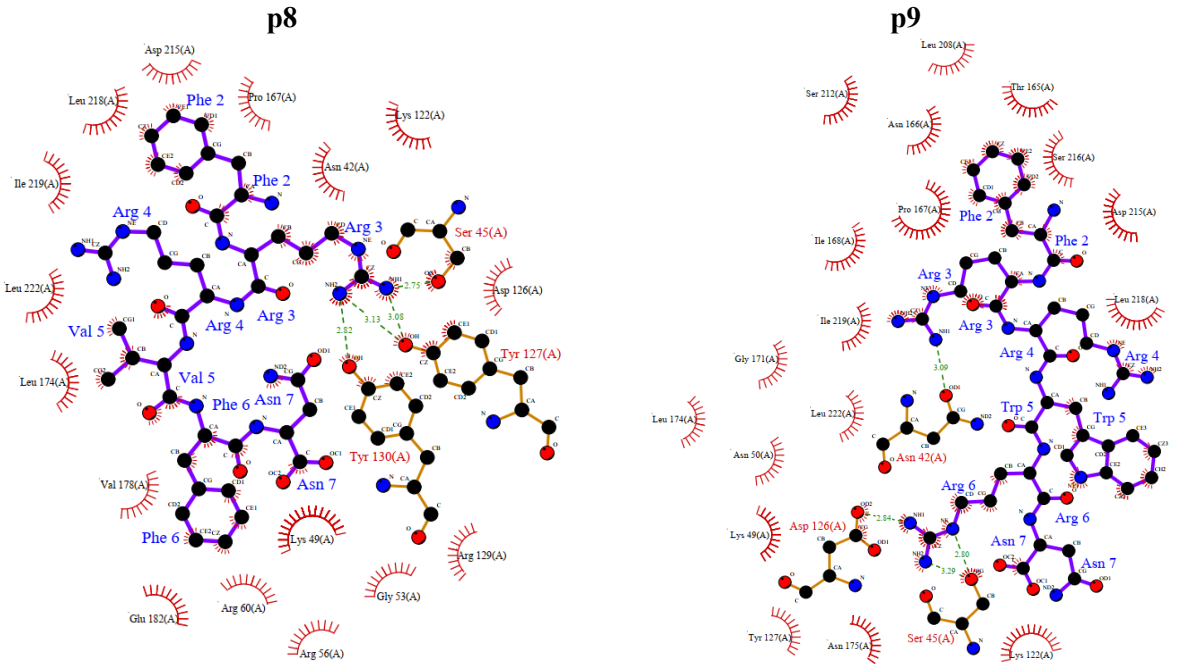


Figure 3. AutoDock Vina predicted the protein-peptide interaction of p8 and p9 with the amphipathic groove of 14-3-3σ. Peptides are labeled with the abbreviation and the number of amino acids in blue font. The green dashed line indicates hydrogen bonds. Orange arcs present the vdW interactions.

MD simulation

To assess the binding mode and stability of the top-ranked peptides in the amphipathic groove, we performed CG-MD simulations for 500 ns and subsequent all-atom MD simulations for 20 ns per complex. The trajectories of the peptide–14-3-3σ complexes were compared to the initial, ligand-free (apo) protein structure. We monitored thermodynamic parameters, such as total binding energy and temperature, as well as structural stability, using RMSD values throughout the simulations. Thermodynamic cycles were analyzed using the slow-growth method in GROMACS 4.6, calculating Helmholtz/Gibbs free energy differences by integrating over λ (from the receptor-only system at λ=0 to the peptide–receptor complex at λ=1) across equilibrium ensembles generated from the MD runs.

Complex stability was evaluated using RMSD analysis. Table 2 summarizes the RSD of RMSD values for both the receptor and peptides. RMSD deviations within the 14-3-3σ binding groove relative to the apo structure were minimal, indicating overall structural stability. Among the nine top-designed peptides, p3 formed the most stable complex, with stability ranked as p3 > p8 > p5 > p6 > p4 > p9 > p1 > p7 > p2 (Table 2).

Binding free energy analysis (Table 2) showed that p5 exhibited the lowest interaction energy (23.16 kJ/mol), whereas p9 showed the highest (80.60 kJ/mol). The interaction energy ranking was p9 > p8 > p1 > p2 > p6 > p3 > p4 > p7 > p5. Overall, p8, p9, and p3 formed the most stable complexes with the highest interaction energies. These peptides engaged more key residues, including Ser45. Per-residue energy analysis further confirmed that p8 and p9 displayed the strongest interactions (−11.78 and −13.43 kJ/mol/residue, respectively). The results indicated that p8 and p9, which exhibited the lowest RMSD values, the highest binding free energies, and

[Downloaded from ajpr.umsha.ac.ir on 2026-11-06]

[DOI: 10.53208/ajpr.6.1.15]

key stabilizing interactions, are promising peptidic modulators for inhibiting 14-3-3σ. Based on binding energy criteria, p8 and p9 showed two of the strongest binding affinities, with values of −70 and −80 kJ/mol, respectively. Both selected hexapeptides contain the FRR motif, while p9 is particularly arginine-rich, comprising three Arg residues. In p9, Arg5 formed three hydrogen bonds with Asp126 and Ser45, and Arg2 interacted with Asn42 via a hydrogen bond. Additionally, from the early stages of the MD trajectory, p9 established key interactions in which Phe2 and Trp5 engaged the amphipathic groove through van der Waals interactions. Both p8 and p9 are arginine-rich, positively charged peptides, which may facilitate efficient cell membrane penetration. Notably, this study represents the first application of a supervised ML–based modeling approach to identify more adaptive and stable anticancer inhibitory peptides targeting the amphipathic site of 14-3-3σ.

Table 2. Relative standard deviation of RMSD for peptide and protein in the predicted complex, total binding energies, and binding energy per residue between the designed peptides (p8 and p9) and 14-3-3σ obtained during MD simulation.

Peptide	RSD of RMSD (%)		Binding energy (Kj.mol^{-1})	Binding energy per residue (Kj.mol^{-1})
	Peptide	14-3-3σ		
p1	21.42	14.54	-47.37	-7.90
p2	28.02	19.39	-43.45	-7.25
p3	8.69	8.64	-39.83	-6.63
p4	21.86	12.89	-38.11	-6.35
p5	17.98	12.32	-23.16	-3.86
p6	20.07	12.84	-39.90	-6.65
p7	25.46	15.17	-37.67	-6.27
p8	17.80	12.09	-70.71	-11.78
p9	20.44	13.31	-80.60	-13.43

While this study focuses on 14-3-3σ, selectivity over other isoforms remains to be experimentally validated. Our design targeted unique residues including Met202, Asp204, and His206, which distinguish 14-3-3σ from other family members.

Synthesis, purification, and identification

The two highest-scoring peptides, p8 and p9, were synthesized using SPPS. In this method, peptide assembly was carried out stepwise on a solid resin support, allowing excess reagents and by-products to be removed by simple washing after each coupling reaction. The Fmoc (9-fluorenylmethoxycarbonyl) strategy was employed to protect the N-terminus during chain elongation. Before adding each new amino acid, the synthesis yield was monitored by measuring the absorbance of the cleaved Fmoc protecting group at 301 nm, enabling real-time assessment of coupling efficiency. The average coupling yield exceeded 70% at each step, indicating efficient peptide elongation. Following synthesis, the peptides were purified by reverse-phase high-performance liquid chromatography (RP-HPLC) and their identities were confirmed by electrospray ionization mass spectrometry (ESI-MS). The purity of the p8 and p9 peptides was analyzed by analytical HPLC. The molecular weight of p8 (MW: 837.46) and p9 (M: 933.51) was confirmed by mass spectrometry analysis, $[M + H]^+$: 838.34 and $[M + H]^+$: 934.49, respectively (Fig. 4).

The results of the MTT assay demonstrated that p9 exhibited significantly higher cytotoxic activity than p8, consistent with their respective IC_{50} values of 12.3±1.7 µM for p9 and 127.1±9.3 µM for p8. A comparative analysis of peptides p8 (FRRVFN) and p9 (FRRWRN) highlights key sequence features governing inhibitory potency. Both peptides share a conserved FRR motif at the N-terminus, suggesting this region is critical for initial recognition and electrostatic anchoring within the 14-3-3σ amphipathic groove, likely through interactions between the positively charged Arg residues and acidic residues of the binding site. The marked enhancement in potency observed for p9 (~10-fold improvement over p11) can be attributed primarily to substitutions at positions 4–6. In p8, Val4 and Phe5 provide limited hydrophobic and aromatic interactions, whereas in p9, Trp4 introduces a bulky aromatic side chain capable of engaging in stronger π–π stacking and hydrophobic contacts within the binding groove. Additionally, the replacement of Phe6 in p8 with Arg5 in p9 introduces a positively charged residue that may participate in ionic and hydrogen bindings, thereby stabilizing the peptide–protein complex. Overall, the SAR indicates that while the FRR motif is essential for activity, a tryptophan residue at position 4 and a polar C-terminal residue significantly enhance binding affinity and inhibitory potency. These findings suggest that increasing aromaticity and hydrogen-bonding capacity in the C-terminal region of FRR-

[Downloaded from ajpr.umsha.ac.ir on 2026-11-06]

[DOI: 10.53208/ajpr.6.1.15]

containing peptides is a key strategy for improving inhibition of 14-3-3σ.

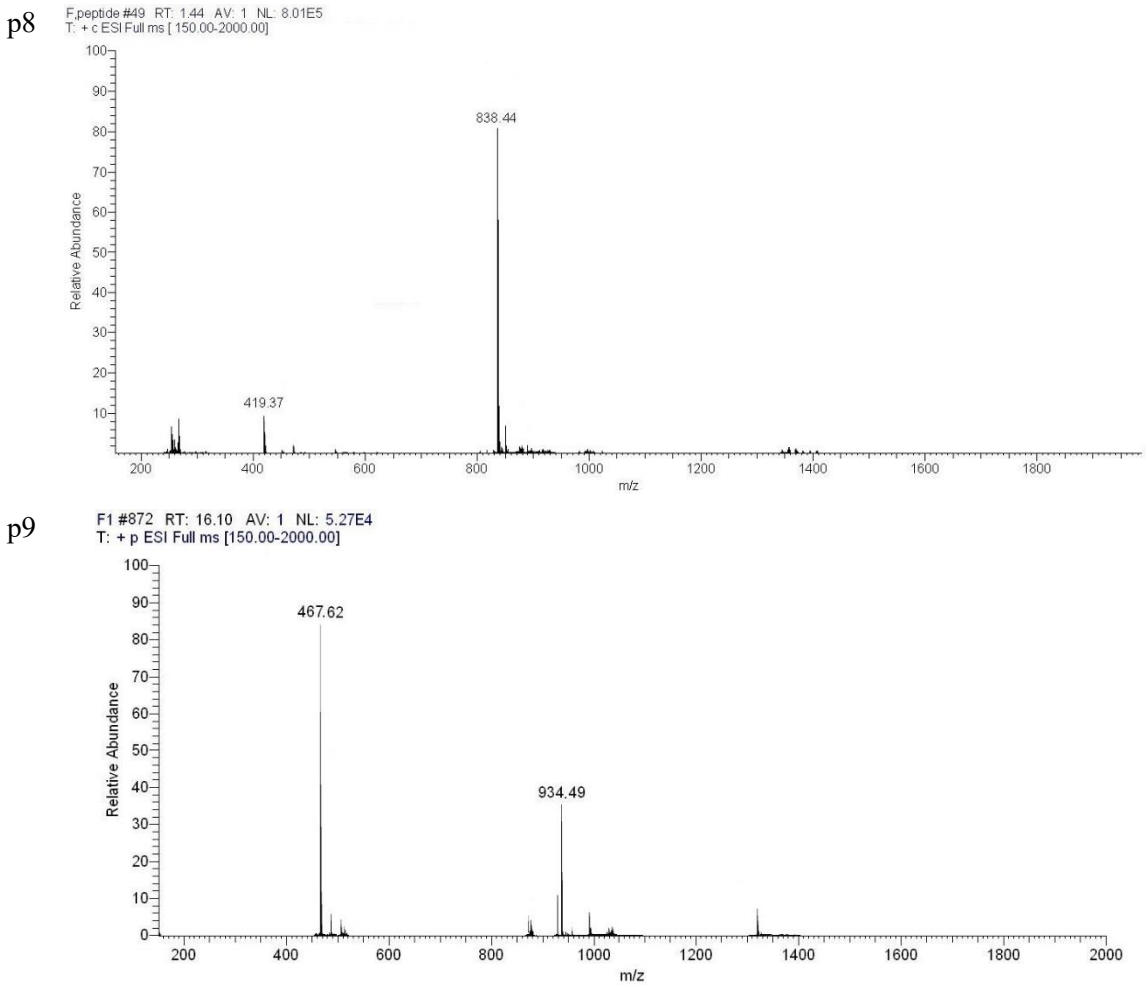


Figure 4. ESI-MS of the two synthesized peptides p8 and p9.

Conclusion

Targeting protein–protein interactions remains challenging; however, recent advances in rational drug design have enabled effective modulation of such targets. Because of its critical role in cancer-related signaling pathways, 14-3-3σ is a valuable therapeutic target, particularly given its isoform-specific dysregulation in malignancies. Peptides are well suited to inhibit 14-3-3σ because of their high affinity and specificity for the amphipathic groove, and recent pharmaceutical developments have addressed their traditional limitations. In the present work, we applied an integrated fragment-based design and supervised ML approach, followed by MD simulations, to identify selective peptidic inhibitors of 14-3-3σ. This strategy enabled efficient screening and optimization of candidate peptides, leading to the identification of p8 (FRRVFN) and p9 (FRRWRN) as the most promising inhibitors. Both peptides formed stable interactions with key residues and exhibited binding and cytotoxicity profiles that were consistent across computational and experimental evaluations. This workflow highlights the effectiveness of combining ML with molecular modeling for the rational design of isoform-specific 14-3-3σ inhibitors. Future studies will include cell uptake experiments, pharmacokinetic profiling, and in vitro efficacy. These investigations are essential to evaluate the efficacy of these peptide candidates.

References

1. van Wier SP, Beekman AM. Peptide design to control protein-protein interactions. Chem Soc Rev. 2025;54(4):1684-98. [DOI: 10.1039/D4CS00243A] [PMID] [PMCID]

[Downloaded from ajpr.umsha.ac.ir on 2026-11-06]

[DOI: 10.53208/ajpr.6.1.15]

2. Zhang J, Humphreys IR, Pei J, Kim J, Choi C, Yuan R, et al. Predicting protein-protein interactions in the human proteome. Science. 2025;390(6771):eadt1630. [DOI: 10.1126/science.adt1630] [PMID] [PMCID]
3. Cierpicki T, Grembecka J. Targeting protein-protein interactions in hematologic malignancies. Annu Rev Pathol. 2025;20(1):275-301. [DOI: 10.1146/annurev-pathmechdis-031521-033231] [PMID]
4. Nibbe RK, Chowdhury SA, Koyutürk M, Ewing R, Chance MR. Protein-protein interaction networks and subnetworks in the biology of disease. Wiley Interdiscip Rev Syst Biol Med. 2011;3(3):357-67. [DOI: 10.1002/wsbm.121] [PMID]
5. Ivanov AA, Khuri FR, Fu H. Targeting protein-protein interactions as an anticancer strategy. Trends Pharmacol Sci. 2013;34(7):393-400. [DOI: 10.1016/j.tips.2013.04.007] [PMID] [PMCID]
6. Nevola L, Giralt E. Modulating protein-protein interactions: the potential of peptides. Chem Commun (Camb). 2015;51(16):3302-15. [DOI: 10.1039/C4CC08565E] [PMID]
7. Giusto E, Yacoubian TA, Greggio E, Civiero L. Pathways to Parkinson's disease: a spotlight on 14-3-3 proteins. NPJ Parkinsons Dis. 2021;7:85.[DOI: 10.1038/s41531-021-00230-6] [PMID]
8. Mhawech P. 14-3-3 proteins—an update. Cell Res. 2005;15(4):228-36. [DOI: 10.1038/sj.cr.7290291] [PMID]
9. Aghazadeh Y, Papadopoulos V. The role of the 14-3-3 protein family in health, disease, and drug development. Drug Discov Today. 2016;21(2):278-87. [DOI: 10.1016/j.drudis.2015.09.012] [PMID]
10. Khorrami A, Sharif Bagheri M, Tavallaei M, Gharechahi J. The functional significance of 14-3-3 proteins in cancer: focus on lung cancer. Horm Mol Biol Clin Investig. 2017;32(3). [DOI: 10.1515/hmbci-2017-0032] [PMID]
11. Falcicchio M, Ward JA, Macip S, Doveston RG. Regulation of p53 by the 14-3-3 protein interaction network: new opportunities for drug discovery in cancer. Cell Death Discov. 2020;6(1):1-21. [DOI: 10.1038/s41420-020-00362-3] [PMID] [PMCID]
12. Aljabal G, Yap BK. 14-3-3σ and Its Modulators in Cancer. Pharmaceuticals. 2020;13(12):441. [DOI: 10.3390/ph13120441] [PMID] [PMCID]
13. Gardino AK, Smerdon SJ, Yaffe MB, editors. Structural determinants of 14-3-3 binding specificities and regulation of subcellular localization of 14-3-3-ligand complexes: a comparison of the X-ray crystal structures of all human 14-3-3 isoforms. Semin Cancer Biol; 2006;16(3):173-82. [DOI: 10.1016/j.semcancer.2006.03.007] [PMID]
14. Stevers LM, Sijbesma E, Botta M, MacKintosh C, Obsil T, Landrieu I, et al. Modulators of 14-3-3 protein–protein interactions. J Med Chem. 2017;61(9):3755-78. [DOI:10.1021/acs.jmedchem.7b00574] [PMID] [PMCID]
15. Huang Y, Yang M, Huang W. 14-3-3 σ: A potential biomolecule for cancer therapy. Clin Chim Acta. 2020;511:50-8. [DOI: 10.1016/j.cca.2020.09.009] [PMID]
16. Ballone A, Centorrino F, Ottmann C. 14-3-3: a case study in PPI modulation. Molecules. 2018;23(6):1386. [DOI: 10.3390/molecules23061386] [PMID] [PMCID]
17. Lee M-H, Lozano G, editors. Regulation of the p53-MDM2 pathway by 14-3-3 σ and other proteins. Semin Cancer Biol. 2006;16(3):225-34. [DOI: 10.1016/j.semcancer.2006.03.009] [PMID]
18. Wolter M, de Vink P, Neves JF, Srdanović S, Higuchi Y, Kato N, et al. Selectivity via cooperativity: Preferential stabilization of the p65/14-3-3 interaction with semisynthetic natural products. J Am Chem Soc. 2020;142(27):11772-83. [DOI: 10.1021/jacs.0c02151] [PMID] [PMCID]
19. Gigante A, Sijbesma E, Sánchez-Murcia PA, Hu X, Bier D, Bäcker S, et al. A Supramolecular Stabilizer of the 14-3-3ζ/ERα Protein-Protein Interaction with a Synergistic Mode of Action. Angew Chem Int Ed. 2020;59(13):5284-7. [DOI: 10.1002/anie.201914517] [PMID] [PMCID]
20. Thiel P, Röglin L, Meissner N, Hennig S, Kohlbacher O, Ottmann C. Virtual screening and experimental validation reveal novel small-molecule inhibitors of 14-3-3 protein–protein interactions. Chem Commun. 2013;49(76):8468-70. [DOI: 10.1039/c3cc44612c] [PMID]
21. Bier D, Rose R, Bravo-Rodriguez K, Bartel M, Ramirez-Anguita JM, Dutt S, et al. Molecular tweezers modulate 14-3-3 protein–protein interactions. Nat Chem. 2013;5(3):234-9. [DOI: 10.1038/nchem.1570] [PMID]
22. Corradi V, Mancini M, Manetti F, Petta S, Santucci MA, Botta M. Identification of the first non-peptidic small molecule inhibitor of the c-Abl/14-3-3 protein–protein interactions able to drive sensitive and Imatinib-resistant leukemia cells to apoptosis. Bioorg Med Chem Lett. 2010;20(20):6133-7. [DOI: 10.1016/j.bmcl.2010.08.019] [PMID]
23. 2Wang B, Yang H, Liu YC, Jelinek T, Zhang L, Ruoslahti E, Fu H. Isolation of high-affinity peptide antagonists of 14-3-3 proteins by phage display. Biochemistry. 1999;38(38):12499-504. [DOI: 10.1021/bi991353h] [PMID]
24. Nim S, Jeon J, Corbi-Verge C, Seo M-H, Ivarsson Y, Moffat J, et al. Pooled screening for antiproliferative inhibitors of protein-protein interactions. Nat Chem Biol. 2016;12(4):275-81. [DOI: 10.1038/nchembio.2026] [PMID] [PMCID]
25. Hellinger R, Vasileva M, Muhammad T, Gunasekera S, Kümmel D, Göransson U, et al. Chemical proteomics for target discovery of head-

[Downloaded from ajpr.umsha.ac.ir on 2026-11-06]

[DOI: 10.53208/ajpr.6.1.15]

to-tail cyclized mini-proteins. Front Chem. 2017;5:73. [DOI: 10.3389/fchem.2017.00073] [PMID] [PMCID]
26. Lee Y, Chung B, Ko D, Lim H-S. A solid-phase method for synthesis of dimeric and trimeric ligands: Identification of potent bivalent ligands of 14-3-3σ. Bioorg Chem. 2019;91:103141. [DOI: 10.1016/j.bioorg.2019.103141] [PMID]
27. Andrei SA, Thijssen V, Brunsveld L, Ottmann C, Milroy LG. A study on the effect of synthetic α-to-β(3)-amino acid mutations on the binding of phosphopeptides to 14-3-3 proteins. Chem Commun (Camb). 2019;55(98):14809-12. [DOI: 10.1039/c9cc07982c] [PMID]
28. Majeux N, Scarsi M, Apostolakis J, Ehrhardt C, Caflisch A. Exhaustive docking of molecular fragments with electrostatic solvation. Proteins. 1999;37(1):88-105. [DOI: 10.1002/(SICI)1097-0134(19991001)37:1%3C88::AID-PROT9%3E3.0.CO;2-O] [PMID]
29. Huang J, MacKerell Jr AD. CHARMM36 all-atom additive protein force field: Validation based on comparison to NMR data. J Comput Chem. 2013;34(25):2135-45. [DOI: 10.1002/jcc.23354] [PMID] [PMCID]
30. Vanommeslaeghe K, Hatcher E, Acharya C, Kundu S, Zhong S, Shim J, et al. CHARMM general force field: A force field for drug-like molecules compatible with the CHARMM all-atom additive biological force fields. J Comput Chem. 2010;31(4):671-90. [DOI: 10.1002/jcc.21367] [PMID] [PMCID]
31. Chauhan M, Gupta A, Tomer R, Raghava GP. CancerPPD2: an updated repository of anticancer peptides and proteins. Database. 2025;2025:baaf030. [DOI: 10.1093/database/baaf030] [PMID] [PMCID]
32. Koch CP, Perna AM, Pillong M, Todoroff NK, Wrede P, Folkers G, et al. Scrutinizing MHC-I binding peptides and their limits of variation. PLoS Comput Biol. 2013;9(6):e1003088. [DOI: 10.1371/journal.pcbi.1003088] [PMID] [PMCID]
33. Eisenberg D, Weiss RM, Terwilliger TC. The helical hydrophobic moment: a measure of the amphiphilicity of a helix. Nature. 1982;299(5881):371-4. [DOI: 10.1038/299371a0] [PMID]
34. Trott O, Olson AJ. AutoDock Vina: improving the speed and accuracy of docking with a new scoring function, efficient optimization, and multithreading. J Comput Chem. 2010;31(2):455-61. [DOI: 10.1002/jcc.21334] [PMID] [PMCID]
35. Marrink SJ, Risselada HJ, Yefimov S, Tieleman DP, De Vries AH. The MARTINI force field: coarse grained model for biomolecular simulations. J Phys Chem B. 2007;111(27):7812-24. [DOI: 10.1021/jp071097f] [PMID]
36. Van Der Spoel D, Lindahl E, Hess B, Groenhof G, Mark AE, Berendsen HJ. GROMACS: fast, flexible, and free. J Comput Chem. 2005;26(16):1701-18. [DOI: 10.1002/jcc.2029] [PMID]
37. Bussi G, Donadio D, Parrinello M. Canonical sampling through velocity rescaling. J Chem Phys. 2007;126(1):014101. [DOI: 10.1063/1.2408420] [PMID]
38. Hess B, Bekker H, Berendsen HJ, Fraaije JG. LINCS: a linear constraint solver for molecular simulations. J Comput Chem. 1997;18(12):1463-72. [DOI: 10.1002/(SICI)1096-987X(199709)18:123.0.CO;2-H]

[Downloaded from ajpr.umsha.ac.ir on 2026-11-06]

[DOI: 10.53208/ajpr.6.1.15]